Coatable xLiI-(1-x)Li_4SnS_4 Solid Electrolytes prepared from Aqueous Solutions for All-Solid-State Lithium-Ion Batteries

Youngeun Choi

Department of Energy Engineering
(Battery Science and Technology)

Graduate School of UNIST

Coatable xLiI-(1-x)Li_4SnS_4 Solid Electrolytes prepared from Aqueous Solutions for All-Solid-State Lithium-Ion Batteries

A thesis/dissertation
submitted to the Graduate School of UNIST
in partial fulfillment of the
requirements for the degree of
Master of Science

Youngeun Choi

1. 11. 2017 Month/Day/Year of submission
Approved by

_____

Advisor
Yoon Seok Jung

Coatable xLiI-(1-x) Li_4SnS_4 Solid Electrolytes prepared from Aqueous Solutions for All-Solid-State Lithium-Ion Batteries

Youngeun Choi

This certifies that the thesis/dissertation of Youngeun Choi is approved.

1/11/2017

signature

_____

Advisor: Yoon Seok Jung

signature

_____

Youngsik Kim

signature

_____

Seok Ju Kang

Abstract

Bulk-type all-solid-state lithium-ion batteries (ASLBs) for large-scale energy storage applications have emerged as a promising alternative to conventional lithium-ion batteries (LIBs) owing to their superior safety. However, the electrochemical performance of bulk-type ASLBs is critically limited by the low ionic conductivity of solid electrolytes (SEs) and poor ionic contact between the active materials and SEs. Herein, we report the highly conductive (0.14 mS cm^{-1}) and dry-air-stable SEs Li_4SnS_4 or LiI-Li_4SnS_4, which are prepared using a scalable aqueous-solution process. An active material ($LiCoO_2$) coated by solidified Li4SnS4 from aqueous solutions results in a significant improvement in the electrochemical performance of ASLBs. Side effect by the exposure of $LiCoO_2$ to aqueous solutions is minimized by using predissolved Li_4SnS_4 solution.

Contents

List of Figures

Figure S4. Raman spectra of LSS-coated $LiCoO_2$. The spectra of LSS320 is also shown for comparison.

Figure S5. HRTEM images of LSS-coated $LiCoO_2$ particle.

Figure S6. Rate capabilities of p-LCO and w-LCO electrodes in liquid-electrolyte cells cycled between 3.0-4.3 V (vs. Li/Li^+).

Figure S7. Rate capability of the 0.4LiI-0.6LSS200-coated $LiCoO_2$ electrode. a) Variations in discharge capacities versus charge-discharge cycle number at different C-rates. b) Discharge voltage profiles at different C-rates. The $LiCoO_2$:0.4LiI-0.6LSS200 weight ratio in the composite electrodes was 85:15. The data for the mixed electrodes and the LSS320-coated $LiCoO_2$ electrodes are also shown for comparison

Nomenclatures

LIBs	Lithium-ion batteries
EVs	Electric vehicles
SEs	Solid electrolytes
ASLBs	All solid-state lithium ion batteries
LGPS	$Li_{10}GeP_2S_{12}$
LPS	Li_3PS_4
LSS	Li_4SnS_4
MeOH	methanol
TGA	Thermogravimetric analysis
XRD	X-ray diffraction analysis
FESEM	Field emission scanning electron microscope
EDXS	Energy dispersive X-ray spectroscopy
HR-TEM	High Resolution Transmission electron microscope
ICP-OES	Inductively coupled plasma optical emission spectroscopy
EIS	Electrochemical Impedance spectroscopy
GITT	Galvanostatic intermittent titration technique
FIB	focused ion beam
p-LCO	pristine $LiCoO_2$
w-LCO	water-treated $LiCoO_2$

1. Introduction

Lithium-ion batteries (LIBs) are commonly used in small-scale applications; however, in recent years they have become increasingly used in large-scale applications such as electric vehicles (EVs).[1] However, safety concerns with LIBs, originating from their use of flammable organic liquid electrolytes, have hindered their widespread commercial application. Accordingly, composite-structured bulk-type all-solid-state lithium-ion batteries (ASLBs) using inorganic solid electrolytes (SEs) have emerged as promising alternatives.[2] In order to achieve performance levels in bulk-type ASLBs that compete with those of conventional LIBs, development of highly conductive SEs is imperative.[2a, 2b, 2e, 3] Several sulfide SEs exhibit extremely high conductivities (e.g., $Li_{10}GeP_2S_{12}$ (LGPS):[2a] 12 mS cm^{-1}, $Li_3P_7S_{11}$:[3] 17 mS cm^{-1}, $Li_{9.54}Si_{1.74}P_{1.44}S_{11.7}Cl_{0.3}$:[2e] 25 mS cm^{-1}) that are comparable to those of organic liquid electrolytes.[4] Considering that SEs are single ionic conductors whereas transference numbers for Li^+ ions in organic liquid electrolytes are low (0.2-0.4),[2b, 2e, 4] ASLBs employing state-of-the-art sulfide SEs may, in theory, outperform conventional LIBs.

Another critical challenge with bulk-type ASLBs is to achieve favorable interfaces between the active material and the SE. High interfacial resistances are observed between sulfide SEs and conventional cathode materials such as $LiCoO_2$. This can be explained by the intrinsically poor oxidation stability of sulfide materials,[5] chemical reactions between sulfide SEs and active materials,[6] the space charge layer model,[7] and lattice mismatch.[7] Fortunately, significant improvements in interfacial stability have been achieved by protective coating of the active materials by metal oxides such as $LiNbO_3$.[2a, 2d, 6] Furthermore, wetting active materials with SEs is critical for high-performance bulk-type ASLBs.[2d, 8] In the case of bulk-type ASLBs that employ oxide SE materials, high-temperature sintering processes are necessary to form contacts between active materials and SEs.[9] However, this can lead to the formation of undesirable by-products at interfaces, resulting in poor electrochemical performance.[9-10] In contrast, sulfide SEs are deformable, which allows efficient two-dimensional contact by simple cold-pressing.[2d, 11] However, full wetting of active materials with sulfide SEs by cold-pressing alone is still limited .[2d, 8, 11b, 12]

To fabricate electrode composite with favorable ionic contacts, reducing size of TiS_2 particle by ball-milling. Rate performance has been improved along decrease of particle size from ~10 μm to 0.1 μm. Small particle size has shortened lithium ion pathway and larger surface area to contact with SEs.[13] Not only ball milling, exfoliation is done for TiS_2 for the same reason. Lithiation is done for reducing the attraction between the layers. Following sonication in water separates the layers to get TiS_2 nanosheets. These sheets have less stacked structure with higher surface area. This leaded to

enhanced rate performance.[14] TiS_2 and Li_2S-P_2S_5 SE is ball-milled to get the electrode composite exhibiting extra lithium ion storage. Ball-milled composite shows around 416 mAh g^{-1} in voltage range of 1.5-3.0 V with great retention. This comes from amorphous Li-Ti-P-S phase through ball milling.[15] These improvements underline the importance of micro-structure of components in electrode composite with favorable interfacial condition.

In this view, forming a direct contact between active material and SE is ideal with high contact area and reduced lithium ion pathway. A pioneering proof-of-concept for direct SE coating of active materials using pulsed laser deposition, and the resulting improvement in ASLB performance, has been reported.[16] The wet chemical preparation of SEs could be one of the most appropriate strategies to realize the above-mentioned concept in a scalable way. However, the selection of effective combinations of SEs and solvents in which the SEs are dissolved without irreversible chemical reaction with the solvents is extremely challenging.[2d, 8, 11b] To date, very few wet chemical systems for the preparation of sulfide SEs have been reported. These include thio-LISICON ($Li_{3.25}Ge_{0.25}P_{0.75}S_4$, 0.182 mS cm^{-1}) and anhydrous hydrazine,[17] Li_3PS_4 (LPS) and tetrahydrofuran[18] (0.16 mS cm^{-1}) or N-methylformamide (0.026 mS cm^{-1}),[19] $Li_7P_2S_8I$ and acetonitrile (0.63 mS cm^{-1}),[20] and Li_6PS_5Cl and ethanol (0.014 mS cm^{-1}).[21] However, none of these systems simultaneously satisfy the multiple criteria required for a scalable solution-based SE-coating process, i.e., high conductivity (at least 0.1 mS cm^{-1}), environmental benignity, and the use of low-cost, low-boiling-point solvents that afford homogeneous solutions.

Another critical issue is that conventional sulfide SEs that contain phosphorus, such as LPS and LGPS, undergo degradation upon exposure to water or dry air,[2d] as do phosphorus-containing Na-ion SEs, such as Na_3PS_4.[12] However, recent reports of the excellent air-stability of Li_4SnS_4 (LSS),[2d, 22] $Li_{4-x}Sn_{1-x}As_xS_4$,[23] and Li_2SnS_3[24] have led to interest in developing alternative Sn-based SEs. The superior dry-air stability of Sn-based SEs to that of phosphorus-based SEs has been explained by reference to the hard and soft acid and base theory.[2d, 8, 23]

Recently, our group reported a novel highly conductive and dry-air-stable Sn-based Li-ion SE, $0.4LiI$-$0.6Li_4SnS_4$ (0.41 mS cm^{-1}), prepared from a homogeneous methanol (MeOH) solution. LiI is introduced to enhance the conductivity with widen framework and favorable polarizability.[2d] ASLBs employing $LiCoO_2$ coated with this SE exhibited excellent performance. Herein, our development of Sn-based SEs is expanded to a solution process for $xLiI$-$(1-x)Li_4SnS_4$ using the most environmentally desirable solvent (water). Various analyses are done with X-ray diffraction (XRD), Raman, and electron microscopes along optimizing the conditions. Its application for SE-coating of active materials

for ASLBs are evaluated through various electrochemical techniques. Further, coating process is modified for the superior performance of coated composite in aqueous environment.

2. Theoretical & Mathematical Development

2.1 Principle of Lithium-ion batteries

Battery is the energy storage system using the oxidation, reduction of the electrode materials. And electrolyte delivers the ions from one electrode to the other. Membrane physically separate electrodes. Otherwise, there will be flow of electricity in battery system resulting increase of temperature, further explosion. Battery can be divided into two types by its rechargeability. One is primary battery which spontaneously convert chemical energy to electric energy. This conversion is irreversible and battery can discharge once. The other is secondary battery and it can be charged and used repetitively. In charging secondary battery, there is reduction of negative electrode by insertion of lithium. There is oxidation of positive electrode by extraction of lithium at the same time. The opposite chemical reaction occurs during discharging.[25]

Generally, lithium ion battery is adopted with high efficiency. Lithium ion battery has outstanding two advantages: 1) Lithium is one of the lightest elements. This enables raising the specific energy density. 2) Lithium itself has lowest redox potential. It is possible to facilitate two electrodes with high voltage difference.

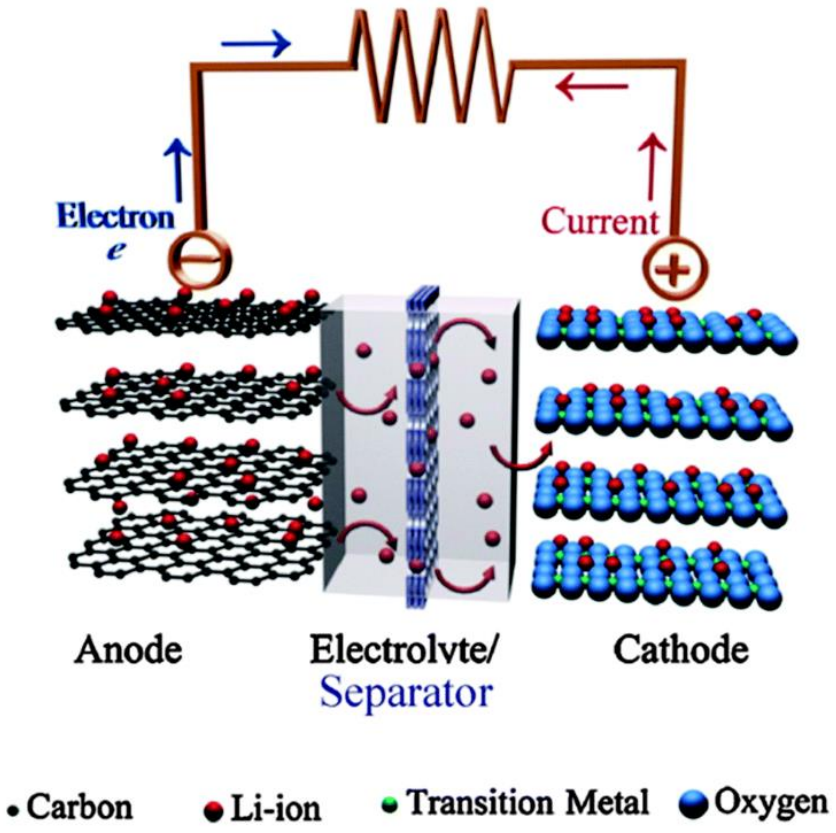

Figure 1. Schematic description of lithium-ion battery with organic liquid electrolyte[26]

2.2 Components in lithium-ion batteries

2.2.1 Cathode

Layered structure

Lithium metal oxides with layered structure show densely stacked crystalline structure with ionic bonding. Oxygen ions have hexagonal close packed or cubic close packed structure and transition metal and lithium ions occupy tetrahedral sites or octahedral sites. Slabs composed of transition metal and oxygen ions with strong ionic bonding. Lithium ions and the slabs are placed by turns. Lithium ions moves along 2 dimensional planes during intercalation and deintercalation for high ionic conductivity.

$LiCoO_2$ is the most widely used cathode material with high power and stable cycle performance. There are irreversible structural changes when more than half of lithium ions deintercalated during charge. The practical specific capacity is around 145 mAh g^{-1} though theoretical specific capacity 274 mAh g^{-1} for $LiCoO_2$ and its average working voltage is 3.9 V.[27]

$LiCoO_2$ has limitations in exhibiting high capacity and disadvantages in toxicity and price. Cobalt is partially substituted to nickel, manganese to overcomes limitations of $LiCoO_2$. Substitution is for higher capacity by nickel, structural stability and low cost by manganese. Stable composition is $LiNi_{1/3}Co_{1/3}Mn_{1/3}O_2$, made up with Ni^{2+}, Co^{3+} and Mn^{4+}. Ni^{2+} mainly participate in charge/discharge and Co^{3+} involves in end of charge. Mn^{4+} placed in octahedral sites and maintain the layered structure stably.[28]

Spinel structure

Oxygen ions are stacked in cubic close packed structure. Transition metals occupies tetrahedral or octahedral sites with various structural variation along synthesizing condition. Spinel structure provides short lithium ion pathway with high ionic conductivity. It enables favorable fast charge/discharge. Most familiar spinel structured cathode material is $LiMn_2O_4$. Manganese has low price with its abundance. However, Jahn-teller distortion and disproportionation reaction by Mn^{3+} is critical issue for $LiMn_2O_4$. Dissolution of Mn^{2+} into electrolyte reduces the amount of active material and hinder transport of lithium ion by electrodeposition.[29]

To eliminate these issues, manganese ion is substituted by transition metal with lower charge or lithium ion. $LiNi_{0.5}Mn_{1.5}O_4$ has high working voltage at 4.7 V with stable cycle performance. This high working voltage is advantageous for achieving high energy density. This leads detrimental side reaction on the other hand. Li[Li, Nm, Co, Ni]O_2 which is also called as over-lithiated layered oxide or Li-excess material can exhibit high capacity of 200-300 mAh g^{-1}. However, it requires high voltage

to activate in charging step. High voltage inevitably result side reaction. Also, it suffers from poor rate performances.[30]

Olivine structure

Cobalt makes $LiCoO_2$ less attractive in cost consideration. Fe is environmentally friendly and cheap with its rich deposits. Strong ionic bonding of polyanion in $LiFeO_4$ reduces strength of covalent bonding between Fe and O. This increases ionic tendency of Fe^{3+}/Fe^{2+} and working voltage to 3.4 V. Its theoretical specific capacity is 170 mAh g^{-1} with structural and chemical stability. Though polyanion enables higher voltage, limits electric conductivity and transport of lithium ion as it can move in one direction.[25]

Li-S

Further, Sulfur is one of the candidates as future active material with its abundance and high theoretical capacity over 1600 mAh g^{-1}. Sulfur have trouble of utilization with its low electric conductivity and dissolution of poly-sulfides (Li_2S_x). Through lithiation and delithiation, there is big changes in volume which leads stresses in electrode structure.

2.2.2 Anode

Lithium

Lithium metal can exhibit high capacity and has lowest voltage which raise the cell voltage. However, the growth of dendrite, the unevenly deposited lithium during repetitive charge, can result the failure of membrane and short circuit. As the direct contact between two electrodes can cause explosion, lithium metal possesses severe safety concern.[31]

Carbon based materials

Carbon based anode materials are divided into two groups, graphitic and non-graphitic carbons. Non-graphitic carbons have small crystalline phase, in disordered structure rather than well stacked structure. Graphite is commercially adopted as anode materials. Graphite has layered structure, and each layer is made up of carbons bonded in hexagon. Electrons can freely move along between the layers, exhibiting high electric conductivity. During charge, lithium intercalates in carbon forming Li_xC. 1 lithium reacts with 6 carbon atoms. Graphite shows stable cycle performance under 0.25 V with theoretical specific capacity of 372 mAh g^{-1}.[1]

Metal alloy

Metal forms alloy with lithium during charge. Alloy becomes metal again with extraction of lithium during discharge. These reactions repetitively occur and are stated below.

$$xLi^+ + xe^- + M \leftrightarrow Li_xM \quad (2\text{-}1)$$

The most promising metal anode material is tin (Sn) and silicon (Si). Especially, Si exhibits high theoretical capacity of 4200 mAh g^{-1}. Also, it is cheap and has adequate working voltage for lithium metal deposition. However, there is extreme volume changes, over 400 %, compared to the initial state. Along volume changes, cracks appear in anode particles. cracks lead exposing additional surface of particle which can be apart from electrolyte. This isolation degrades the performance. [32]

2.2.3 electrolyte

Electrolyte is mediate of lithium transport as mixture of solvents and lithium salt. It delivers lithium from positive to negative electrode during charge, and from negative to positive during discharge. the performance of electrolyte is importance key in performance of lithium ion battery. For lithium salt, it should be dissolved in organic solvent homogeneously without toxicity and corrosiveness. Complex anion, bigger than Li ion is paired for dissolution. $LiPF_6$ is the only salt satisfying the requirements. Linear carbonate and cyclic carbonate species are used for organic liquid solvent for electrolyte. Cyclic carbonates have high dielectric constant dissolving salt easily. Although linear carbonates cannot dissolve salts with low dielectric constant, it can enhance ionic conductance with low viscosity. Commercial liquid electrolyte is $LiPF_6$ dissolved in the mixture of linear and cyclic carbonates in proper ratio. Additives are included for forming stable interface to improve the performance of lithium ion battery.

Ionic liquid is promising candidate as liquid electrolyte. It has wide operating voltage range up to 5.3 V. And inflammability and thermal stability is attractive in safety consideration. However, it is unstable at low voltage under 1.1 V.

2.3 All-solid-state lithium-ion batteries

The organic liquid electrolyte is adopted for utilize the lithium ion battery at high voltage, instead of aqueous liquid electrolyte. However, liquid electrolytes possess flammability and show gas evolution at high temperature which limits applicable condition for lithium ion batteries. These flaws should be considered seriously in larger devices like electric vehicles or energy storage system. Solid electrolyte for ASLBs have competitive advantages with ultimate safety by adopting inorganic solid electrolyte. Thin type ASLBs is fabricated through vacuum deposition process, with high expense. This limits the practical application for larger sized battery. Bulk type ASLBs, all elements composed of solid particles, is ideal for commercialization of ASLBs. There are 3 layers in bulk type ASLBs, 2 electrode layers at each end and SE layer in the middle. Schematic description showing the structure of ASLBs are shown in figrue1. Electrodes are mixture of active material and SE and conductive additives with necessity. High energy density can be achieved by simply stacking cells without additional packing system as there is no worries about leakage. As all components are solids, ionic pathway should be formed through fabrication. Therefore, the performance of SEs, such as ionic conductivity and deformability, strongly determines the performance of ASLBs.

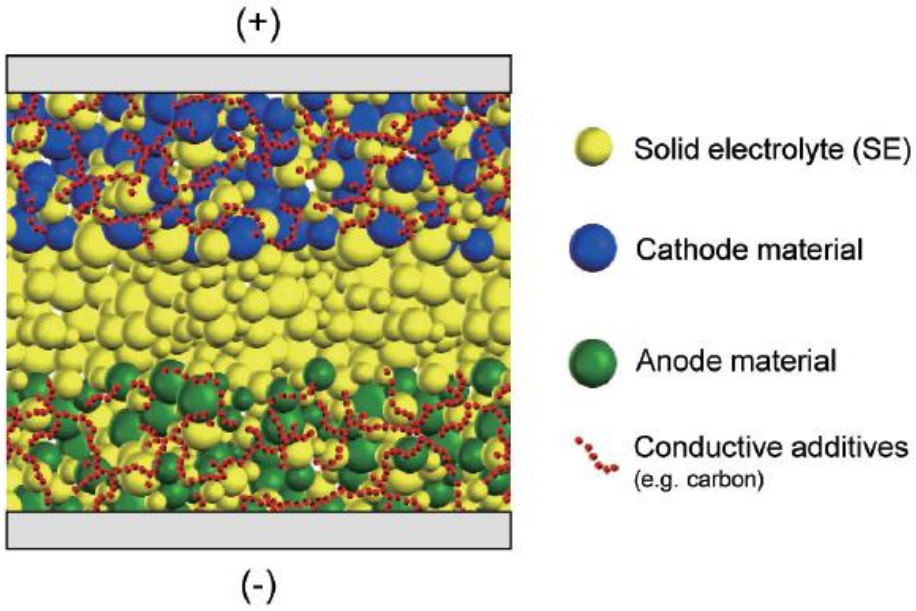

Figure 2. Schematic description of bulk type ASLBs [3]

2.3.1 Inorganic solid electrolyte

Oxide solid electrolyte

Typical oxide solid electrolytes are $Li_{3x}La_{2/3-x}TiO_3$ (LLTO)[33] with perovskite structure, $Li_7La_3Zr_2O_{12}$ (LLZO)[34] with garnet structure, and $Li_{1+x}Al_xTi_{2-x}(PO_4)_3$[35] with NASICON structure. Ionic conductivity of oxide solid electrolytes is in range of 10^{-4}-10^{-3} S cm^{-1}. Oxide SEs are stable in high voltage and air exposure. Its brittleness results large grain boundary resistance and require sintering process at high temperature. Heat treatment occurs volatilization of lithium, phase transition and formation of unwanted impurities. In case of LLTO, lithium metal reduces Ti^{4+} around 1.8 V. LLZO requires high temperature of 1200 ^oC for sintering.

sulfide solid electrolyte

Sulfide SEs are more suitable for bulk type ASLBs without heat treatment and side reactions from it. Sulfide SEs have high deformability allowing cold pressing to form ionic contacts. Furthermore, sulfide SEs have higher conductivity than oxide SEs. These come from larger radius of sulfur ion than oxygen ion with higher polarizability.

Starting from the development of $Li_{3.25}Ge_{0.25}P_{0.75}S_4$ with 2.2 mS cm^{-1} at 25 ^oC, solid electrolytes with high ionic conductivity competitive to liquid electrolytes have been explored.[36] Li_2S-GeS-P_2S_5 system is further studied to achieve high ionic conductivity of 12 mS cm^{-1} in composition of $Li_{10}GeP_2S_{12}$ (LGPS).[2a] $Li_{10}SnP_2S_{12}$ is also synthesized by substituting Ge into Sn. It has lower ionic conductivity, 4 mS cm^{-1} at 27 ^oC, but ideal with low cost. Li_2S-P_2S_5 system also developed actively. They are prepared through high energy ball-milling and following heat treatment. $Li_3P_7S_{11}$ reached high ionic conductivity of 17 mS cm^{-1}.[3] Further, composition by substituting P to Si and introducing halide ions, $Li_{9.54}Si_{1.74}P_{1.44}S_{11.7}Cl_{0.3}$, reached even higher conductivity of 25 mS cm^{-1}.[2e] Sn based sulfide SEs are also researched. Li_4SnS_4 has ionic conductivity of 0.071 mS cm^{-1} at 20 ^oC.[2d, 22] ionic conductivity has been raised up to 1.39 by introducing As, composition to be $Li_{3.833}Sn_{0.833}As_{0.166}S_4$.[23] Sulfide SEs release harmful gas, H_2S with exposure to air. Though decrease in ionic conductivity of phosphorous sulfide SEs is severe, Sn based sulfide SEs are relatively stable in air. This stability is explained in hard and soft acid and base theory. This theory explains the stability of compounds. 'Hard' stands for small and high charged ions and 'soft' for large and low charged ions. And hard/soft acid tend to react with hard/soft base. As Sn is soft acid, it is less affected by oxygen which is hard base.[2d, 8, 23]

In perspective of performance of sulfide SEs in ASLBs, compatibility with active material and its electrochemical stability is important issue. Commercial lithium metal oxides which is used for LIBs

can be adopted as active material for ASLBs. Some of sulfide SEs are irreversibly oxidized at high voltage over 3 V, resulting large loss of capacity during charge.[37] Also, there is poor compatibility between lithium metal oxides and SEs. The diffusion of Co from $LiCoO_2$ and S from Li_2S-P_2S_5 SE are observed between them. The diffusion of ions is elucidated with space charge layer theory and difference of chemical potential. The diffusion forms lithium deficient layer with detrimental effect on performance. $LiNbO_3$, $Li_4Ti_5O_{12}$, Li_2SiO_3, Al_2O_3 coating on active material is tried to prohibit the degradation.[37-38]

3. Experimental Section

3.1 Preparation of materials.

Crystalline Li_4SnS_4 powders as precursors for the aqueous-solution process were prepared by conventional solid-state synthesis, and named as "SS-LSS". A stoichiometric mixture of Li_2S (99.9%, Alfa Aesar), elemental tin (99.8 %, Alfa Aesar), and elemental sulfur (99.5 %, Alfa Aesar) was heat-treated at 650 °C for 24 h in a quartz ampoule sealed under vacuum. After the as-prepared Li_4SnS_4 powders and LiI (99.95%, Alfa Aesar) were dissolved into deionized water, undissolved impurities were removed by filtration. After the filtered solution was subjected to under vacuum and the subsequent heat-treatment at designated temperatures under vacuum, the final powder samples were obtained. The Li_4SnS_4- and 0.4LiI-0.6Li_4SnS_4-coated $LiCoO_2$ powders were prepared by the same aqueous-solution process in the presence of $LiCoO_2$ powders with a heat treatment temperatures of 320 °C and 200 °C, respectively (Figure 1). The $LiNbO_3$-coated $LiCoO_2$ powders were used for the Li_4SnS_4- or 0.4LiI-0.6Li_4SnS_4-coating.[2d, 11b] LPS powders were prepared by the mechanochemical method. A stoichiometric mixture of Li_2S and P_2S_5 (99 %, Sigma Aldrich) was ball-milled at 500 rpm for 10 h and subsequently heat-treated at 243 °C for 1 h in a glass ampoule sealed under vacuum.[2d] LGPS powders were prepared by heat-treatment of a stoichiometric mixture of Li_2S, P_2S_5, and GeS_2 (99.9 %, American Elements) at 550 °C for 12 h in a quartz ampoule sealed under vacuum.[2d]

3.2 Materials characterization.

The thermogravimetric analysis (TGA) experiment was conducted from 30 °C to 300 °C at 5 °C min^{-1} using a SDT Q600 (TA Instrument Corp.) under a flow of Ar. For X-ray diffraction (XRD) measurement, samples were loaded on the XRD holder and sealed under beryllium window for inhibition of air-exposure. D8-Brker Advance Diffractometer (Cu K_α radiation is 1.54056 Å) was used at 40 kV and 40 mA at 15° min^{-1}. Field emission electron microscopy (FESEM) images and the corresponding energy dispersive X-ray spectroscopy (EDXS) elemental maps were obtained using S-4800 (Hitachi Corp.). High resolution electron microscopy (HRTEM) images and the corresponding EDXS elemental maps were obtained using JEM-2100 (JEOL). The elemental composition of aqueous–solution processed SEs and the weight fraction of SEs coated on $LiCoO_2$ were determined by inductively coupled plasma optical emission spectroscopy (ICP-OES) using 720-ES (Varian Corp.). For the dry-air-stability test, 100 mg of SE powders was kept under a flow of dry air (a mixture 21:79 vol. ratio) for 24 h.

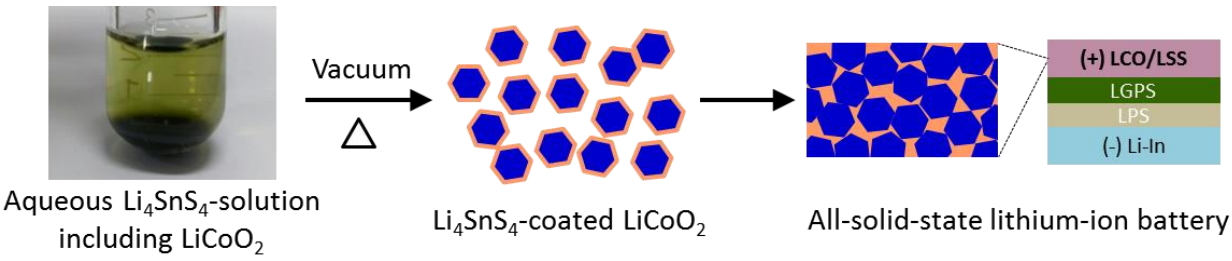

Figure 3. Schematic illustrating the aqueous-solution process for Li_4SnS_4-coated $LiCoO_2$ for ASLBs

3.3 All-solid-state cells.

Composite electrodes were prepared from the $LiCoO_2/Li_4SnS_4$ mixture electrode or the Li_4SnS_4-(or $0.4LiI\text{-}0.6Li_4SnS_4$-) coated $LiCoO_2$. The weight ratio of $LiCoO_2$ and SE was 85:15. All-solid-state cells were fabricated in a 13-mm-diameter polyaryletheretherketone mold. After LGPS/LPS bi-layer film consisting of 120 mg of LGPS and 30 mg of LPS powders was formed by pelletizing, 15 mg of the as-prepared composite electrodes was put on the LGPS-side and spread evenly. Then, 100 mg of $Li_{0.5}In$ which was prepared by mixing In (99%, Sigma-Aldrich) and Li (FMC Lithium Corp.) powders was spread on the LPS-side of LGPS/LPS bilayer. Finally, the cell was pressed under 370 MPa. The galvanostatic charge-discharge cyling of all-solid-state cells was carried out in a voltage range of 3.0-4.3 V (V vs. Li/Li^+) at 30 ^oC. The electrochemical impedance spectroscopy (EIS) measurements were carried out from 1.5 MHz to 5 mHz with amplitude of 10 mV, using the cells charged to 30 mA h g^{-1} at 0.1C and rested for more than 3 h. 1C-rate corresponds with 1.1 mA cm^{-2}. The galvanostatic intermittent titration technique (GITT) measurements were carried out with the pulse of 0.5C for 60 s and rest for 2 h.

4. Results and discussion

The XRD pattern of crystalline Li_4SnS_4 (SS-LSS) (Figure 2a) matches well with that of orthorhombic Li_4SnS_4 with the space group *Pnma*.[22] The as-prepared SS-LSS powder was dissolved in deionized water, forming a transparent greenish-yellow solution (Supporting Information Figure S1). Figure 3 shows the TGA profile of the solid $Li_4SnS_4 \cdot xH_2O$ powder obtained from the as-prepared solution by treatment under vacuum at room temperature. Weight loss is evident at around 150 °C; thus, heat treatment temperatures of 200, 240, 280, 320, and 450 °C were selected to obtain the final samples. Hereafter, the aqueous-solution-processed samples of $xLiI\text{-}(1\text{-}x)Li_4SnS_4$ heat-treated at a given temperature of y (°C) are referred to as "xLiI-(1-x)LSSy".

Figure 2a displays the XRD patterns of the aqueous-solution-processed LSS samples heat-treated at different temperatures. The XRD patterns show amorphous features up to heat-treatment temperatures of 320 °C. Crystalline peaks appear for LSS450 without any noticeable impurity phases. Despite their distinct difference in XRD crystallinities, the Raman spectra of LSS450 and LSS320 both show strong peaks centered at 345 cm^{-1} originating from SnS_4^{4-} (Supporting Information Figure S2).[2d]

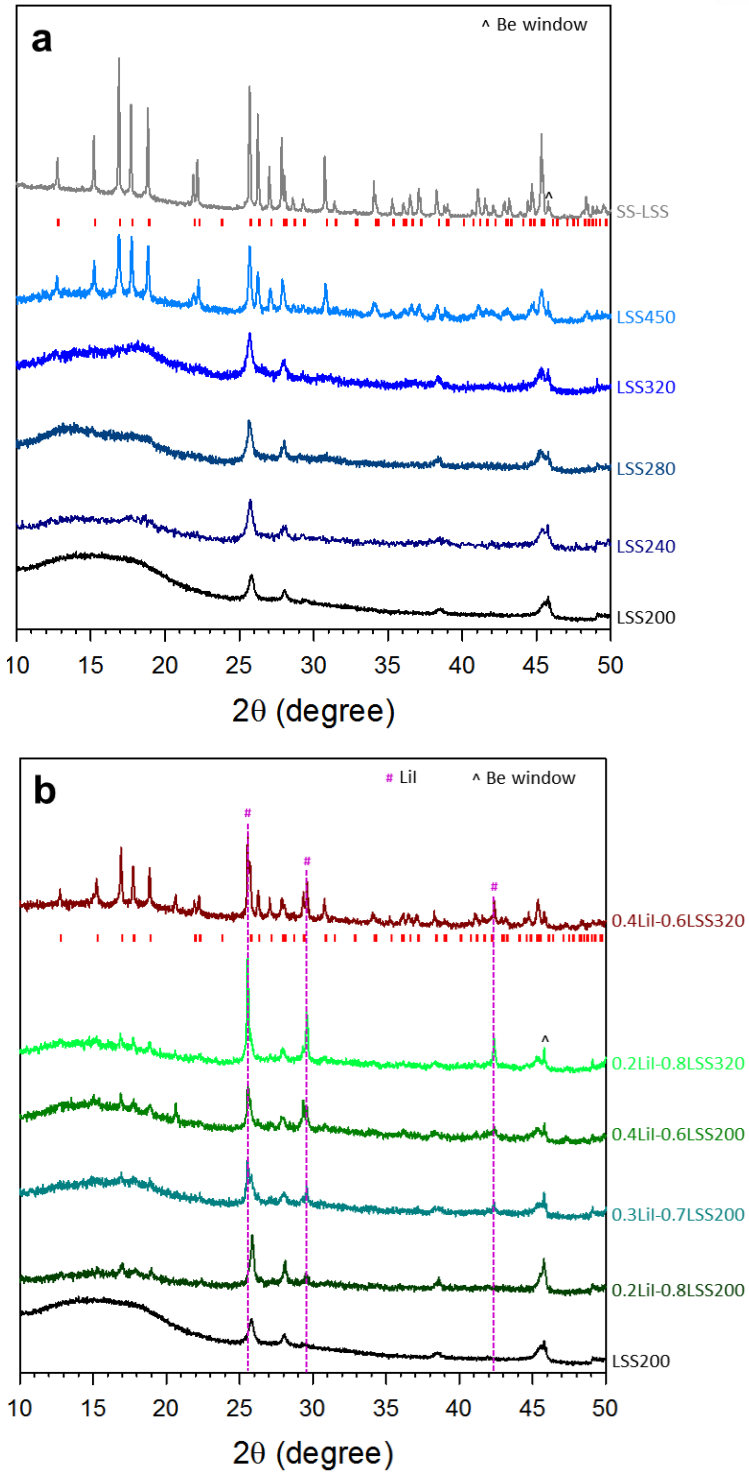

Figure 4. XRD patterns of aqueous-solution processed a) Li_4SnS_4 (LSS) and b) LiI-Li_4SnS_4 (LiI-LSS). The Bragg position for orthorhombic Li_4SnS_4 is marked.[5,26]

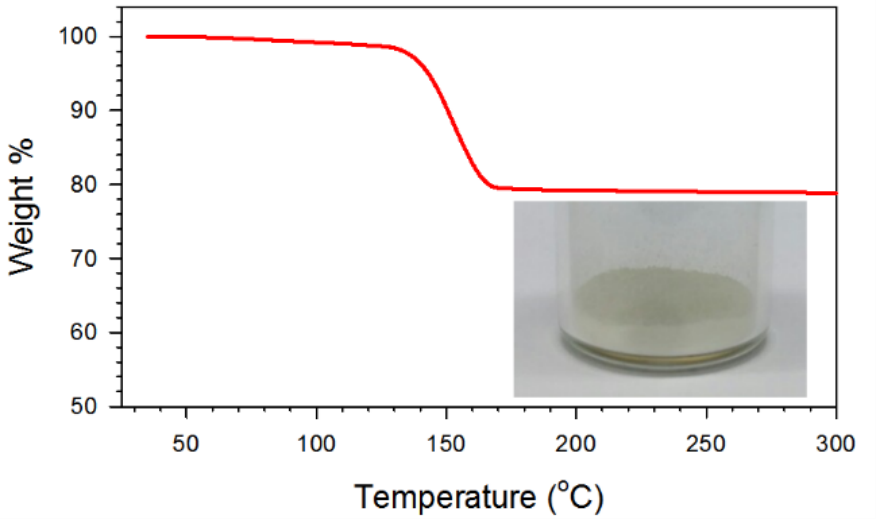

Figure 5. TGA profile of the powder obtained by drying the aqueous Li_4SnS_4 solution under vacuum at room temperature. A photograph of the Li_4SnS_4 powder prepared from aqueous solution with a heat-treatment temperature of 200 °C is shown in the inset.

The ionic conductivities of the solution-processed LSS samples at 30 °C (Figure 4a) show a gradual increase as the heat-treatment temperature increases to 320 °C (LSS320), reaching the maximum value of 0.14 mS cm^{-1}. The conductivity of highly crystalline LSS450 is one order of magnitude lower (0.014 mS cm^{-1}), which agrees well with our previously reported results for MeOH-solution-processed Li_4SnS_4.[2d] Crystalline LSS450 may exhibit poorer deformability than the XRD-amorphous samples (e.g., LSS320), resulting in higher grain boundary resistances in the cold-pressed pellet.[2d]

The XRD patterns of the aqueous-solution-processed LiI-LSS samples are shown in Figure 2b. In all the LiI-LSS samples, especially those prepared at the low heat-treatment temperature of 200 °C, very weak peaks attributed to Li_4SnS_4 are observed. Moreover, all the LiI-LSS samples show characteristic peaks attributed to LiI (JCPDS no. 71–3746). These observations do not agree with our previous results for MeOH-solution-processed LiI-Li_4SnS_4 samples, for which no peaks from crystalline Li_4SnS_4 nor from crystalline LiI (up to x = 0.3 in xLiI-(1-x)Li_4SnS_4) were observed.[2d] These discrepancies emphasize the role of the solvent in solution chemistry in terms of nucleation and growth of crystals.[39] Furthermore, there is a possibility that the use of different precursors (Li_2S and SnS_2 for the MeOH-solution process,[2d] Li_2S, Sn, and S for the aqueous-solution process presented in this work) may result in slight differences in the amounts of impurities and/or stoichiometry, which in turn affect the crystallinity. It is surprising that, despite the observation of segregated crystalline Li_4SnS_4 and LiI, the ionic conductivities of all the LiI-LSS200 samples (e.g., 0.10 mS cm^{-1} for 0.4LiI-0.6LSS200) are higher than that of the LiI-free sample (LSS200, 0.061 mS cm^{-1}), which demonstrates the beneficial role of I^- ions.[2d] Although the elucidation of the underlying mechanism is beyond the experimental limits of the current work, it could be hypothesized that their presence induces i) the improved deformability of LiI-LSS over that of LSS,[2d, 11a] ii) the possible presence of beneficial amorphous regions in which I^- and SnS_4^{4-} form a disordered matrix of mixed anions,[2d] and iii) a possible enhancement of Li-ion transport at Li_4SnS_4/LiI interfaces by formation of a space-charge zone.[40] The higher ionic conductivity of a LiI/Al_2O_3 composite (40 mol% of Al_2O_3: 1×10^{-5} S cm^{-1}) than that of pure LiI (1×10^{-7} S cm^{-1}) has been ascribed to an increase of charge-carrier concentration in a space-charge layer at the interface.[40a] Importantly, in line with previous reports,[2d, 23-24] the aqueous-solution-processed Li_4SnS_4 appears to be stable upon exposure to dry air. LSS320 shows a marginal decrease in conductivity after exposure to dry air for 24 h (0.11 mS cm^{-1}) (Supporting Information Figure S3).

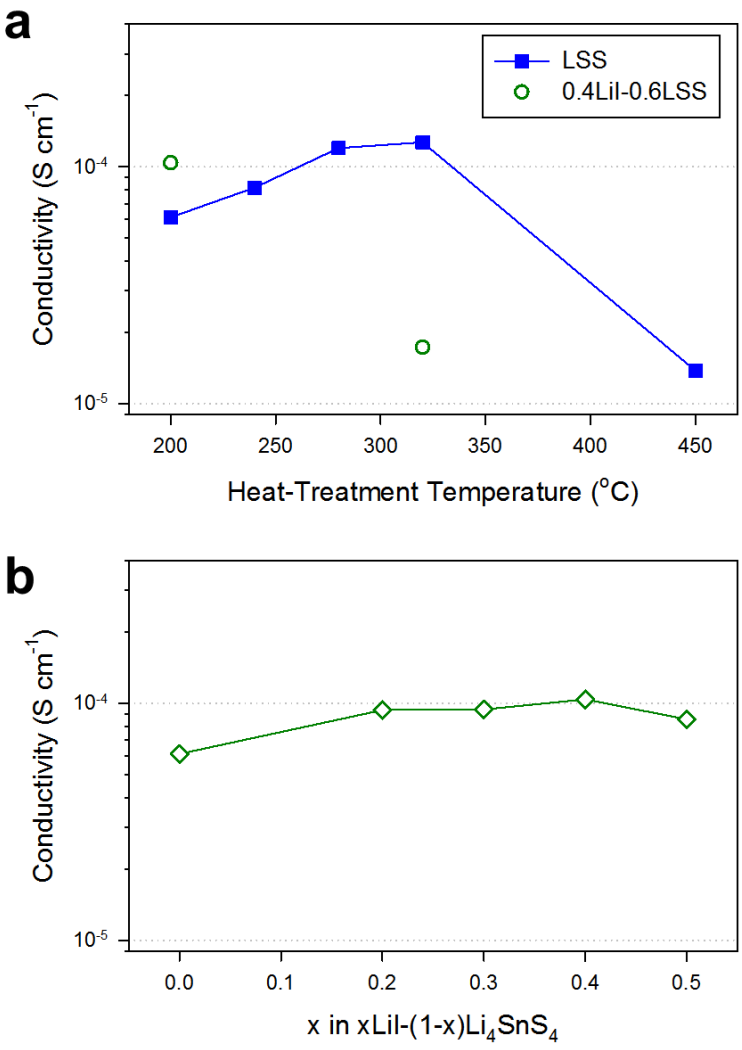

Figure 6. Ionic conductivities of aqueous-solution processed a) LSS as a function of heat-treatment temperature and b) LiI-LSS prepared at 200 °C varied by x in xLiI-(1-x)Li_4SnS_4. The conductivity values were obtained at 30 °C.

The as-developed aqueous-solution process was applied to SE-coating of the active material $LiCoO_2$. Figure 1 illustrates the process of SE-coating and its application to $LiCoO_2$/Li-In all-solid-state cells. Figure 5a shows an FESEM image of an LSS-coated $LiCoO_2$ particle (15 wt% of LSS) and its corresponding EDXS elemental maps, which indicate that the SE layers cover the $LiCoO_2$ particle well. The Raman spectrum of the LSS-coated $LiCoO_2$ powder is almost identical to that of LSS320 (Supporting Information Figure S4). HRTEM images and the corresponding EDXS elemental maps of a focused ion beam (FIB)-cross-sectioned LSS-coated $LiCoO_2$ particle (Figure 5b and Supporting Information Figure S5) highlight the intimate contact between the LSS coating layer and the $LiCoO_2$. Contrary to the XRD-amorphous features of LSS320 (Figure 2a), the coated LSS layer exhibits glass-ceramic-like features with nanocrystallites (Supporting Information Figure S5), which is consistent with our previous results.[2d] The interlayer spacing values obtained from the lattice fringes correspond with those for Li_4SnS_4 (Supporting Information Figure S5b).

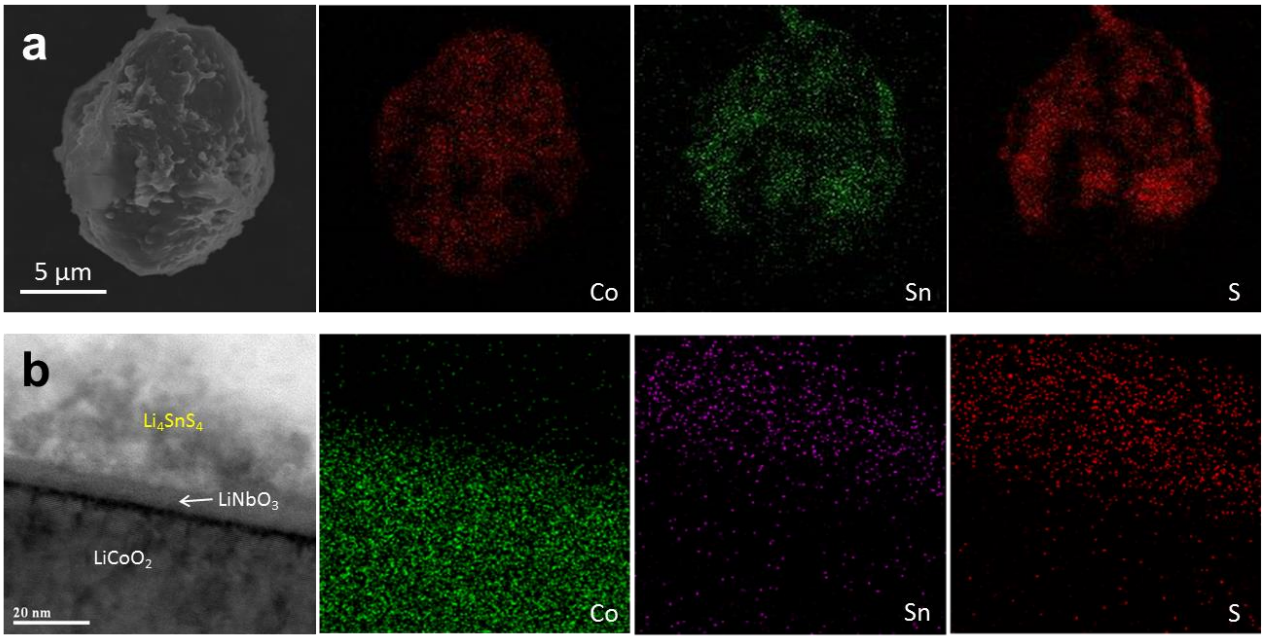

Figure 7. Electron microscopy images of LSS-coated $LiCoO_2$ particles obtained by the aqueous-solution process. a) FESEM image of an LSS-coated $LiCoO_2$ particle and its corresponding EDXS elemental maps. b) HRTEM image of an FIB-cross-sectioned LSS-coated $LiCoO_2$ particle and its corresponding EDXS elemental maps.

The positive composite electrodes of $LiCoO_2$/Li-In all-solid-state cells were fabricated either by manually mixing $LiCoO_2$ and SE (LSS320) powders or by using LSS- or 0.4LiI-0.6LSS-coated $LiCoO_2$ powders. A bilayer SE in which LGPS (6.0 mS cm^{-1}) and LPS (1.0 mS cm^{-1}) are in contact with the $LiCoO_2$ and Li-In electrodes, respectively, was employed in order to maximize the rate capability while avoiding degradation of LGPS at low voltage.[5 2d] Two different LSS-coated $LiCoO_2$ powder samples were prepared, one by mixing $LiCoO_2$ and LSS320 powders in deionized water (referred to as "Coated1"), and one by adding $LiCoO_2$ powder to a predissolved Li_4SnS_4 solution (referred to as "Coated 2"). For fair comparison with the LSS-coated $LiCoO_2$, accordingly, two kinds of $LiCoO_2$ for the mixed electrodes were used; pristine $LiCoO_2$ (p-LCO) and water-treated $LiCoO_2$ (w-LCO). The w-LCO sample was prepared by immersing $LiCoO_2$ powders into deionized water overnight followed by dehydration at 320 °C under vacuum.

The electrochemical performances of the mixed and coated electrodes are shown in Figure 6. As compared to the mixed electrode using p-LCO, the coated electrodes exhibit significant improvements in rate capability. The coated electrodes retain 71% capacity (97 mA h g^{-1}) for Coated1 and 64% (79 mA h g^{-1}) for Coated2 at 1C as compared to that at 0.1C, which is in contrast to the 40% (54 mA h g^{-1}) for the mixed electrode using p-LCO. However, considering that the $LiCoO_2$ used for the coated electrodes was in contact with an aqueous environment during the solution process, a more relevant comparison can be made by comparing the results with those of the mixed electrode made using w-LCO. Surprisingly, the mixed electrode made using w-LCO shows a much poorer rate capability than that of the mixed electrode made using p-LCO, implying the detrimental effect of exposure to water. It is known that surface impurities such as Li_2O, LiOH, and Li_2CO_3 are formed when $LiMO_2$ (M = Co, Ni, Mn) materials are exposed to water or ambient air.[41] The severe degradation in rate capability of the mixed electrode made using w-LCO compared to that of the electrode made using p-LCO is thus explained by contamination of the surfaces.[11b] This observation also agrees with the degradation in rate capability of $LiCoO_2$ upon exposure for conventional LIB cells using liquid electrolytes (Supporting Information Figure S6). The slightly better rate performance for Coated2 than that for Coated1 indicates that side reactions at the surface of $LiCoO_2$ are less severe in the predissolved Li_4SnS_4 solution than in water. Overall, considering this negative effect of the exposure of $LiCoO_2$ to aqueous solutions, the superior rate capability of the aqueous-solution-processed LSS-coated $LiCoO_2$ electrode to that of the mixed electrode made using p-LCO demonstrates the importance of ionic contact between the SE and active materials in ASLBs.[11b, 12] It is believed that the development of a functional protective coating to minimize side reactions occurring in the aqueous solution can further improve the performance,[42] and that adopting alternative eletrode materials that are compatible with aqueous

environments[43] can leverage the advantage of aqueous-soltion-processable Sn-based SEs, which will be the subjects of our next studies.

As shown in Figure 6c, the Coated2 electrode cycled in the voltage range of 3.0-4.3 V (vs. Li/Li^+) at 0.5C exhibits stable cycling performance.

Consistent with the trend of rate capability illustrated in Figure 6a, the discharge voltage profiles at different C-rates indicate higher polarization in the order of the mixed electrode made using w-LCO, the mixed electrode made using p-LCO, and the coated electrodes (Figure 6b).

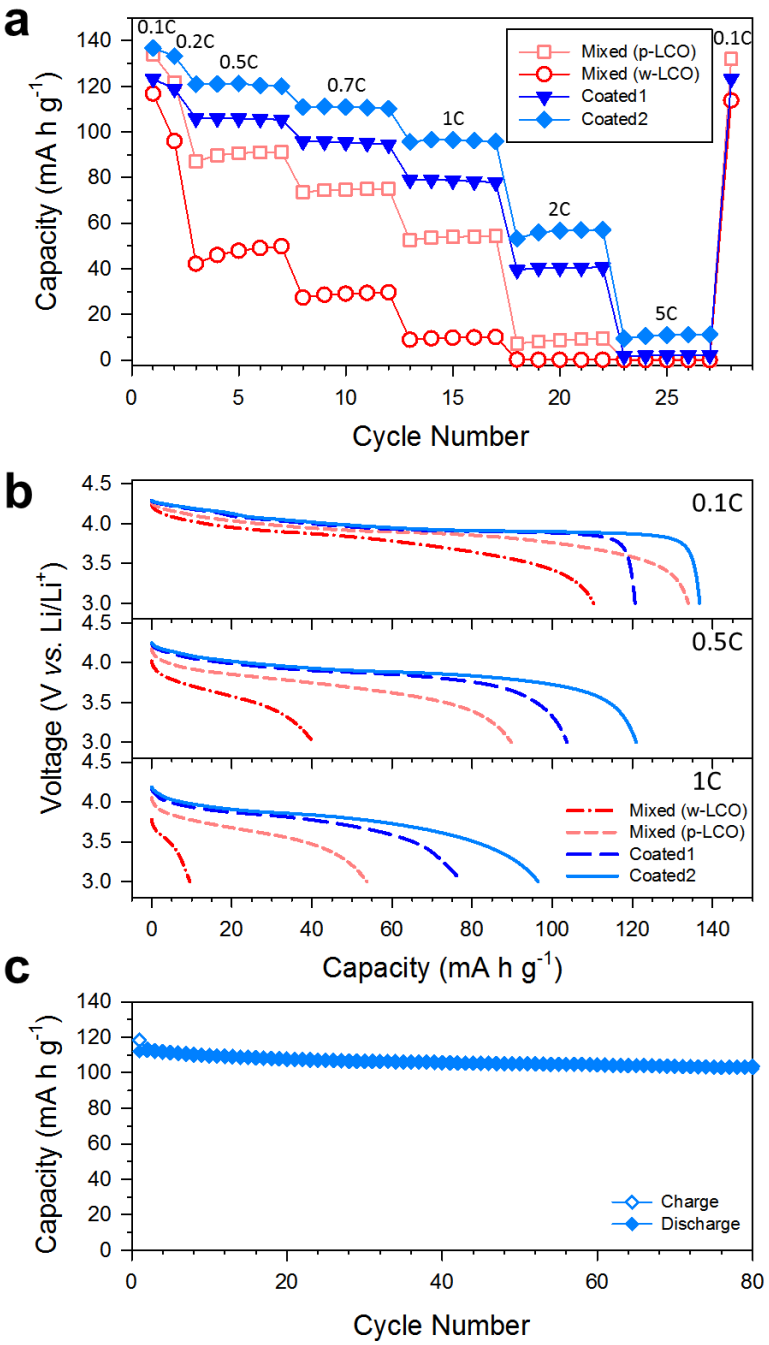

Figure 8. Electrochemical performances of the mixed electrodes and the LSS-coated $LiCoO_2$ electrodes cycled in a voltage range of 3.0-4.3 V (V vs. Li/Li^+). a) Variations in discharge capacities versus charge-discharge cycle number at different C-rates. b) Discharge voltage profiles at different C-rates. c) Cycle performance of the LSS-coated $LiCoO_2$ electrode (Coated2). "p-LCO" and "w-LCO" indicates pristine and water-treated LCO, respectively. The $LiCoO_2$:LSS weight ratio in the composite electrodes was 85:15.

In an attempt to deconvolute the contributions to the overall rate capabilities, the Nyquist plots were compared (Figure 7a). The spectra show one or more semicircles at higher frequency, followed by the Warburg tails at lower frequency. The intercept at the *x*-axis is assigned to the resistance of LGPS/LPS bilayer SE.[2d] The semicircles are interpreted as being due to the contributions of interfacial charge-transfer and electronic resistancies.[2d, 5, 44] The order of the overall amplitude of the semicircles in Figure 7a (ca. 180 Ω for the w-LCO-mixed electrode > ca. 110 Ω for the p-LCO-mixed electrode > ca. 20 Ω for the coated electrodes) agrees perfectly with the results for rate capability (Figure 6a, b). The evolution of mid-frequency semicircles denoted as '#' for the mixed electrode made using w-LCO and for the Coated1 electrode is assigned to the contribution by the surface impurities formed in aqueous environments. The absence of a mid-frequency semicircle for Coated2 confirms the superior stability of $LiCoO_2$ in the predissolved Li_4SnS_4 solution to that in water. Most importantly, it should be noted that the amplitude of the semicircles is also dependent on the interfacial contact area between the active materials and SEs. Thus, the much smaller semicircles for the coated electrodes than those for the mixed electrodes imply intimate ionic contact. Figure 7b compares the GITT voltage profiles for the mixed electrode made using w-LCO and the Coated1 electrode, and their corresponding polarization plots, which again confirms the dramatic improvement by direct SE coating of the active material. The interfacial contact areas between the SE and $LiCoO_2$ were also derived from the GITT curves,[2d, 45] and are much higher for the coated electrode (50%) than for the mixed electrode (23%).

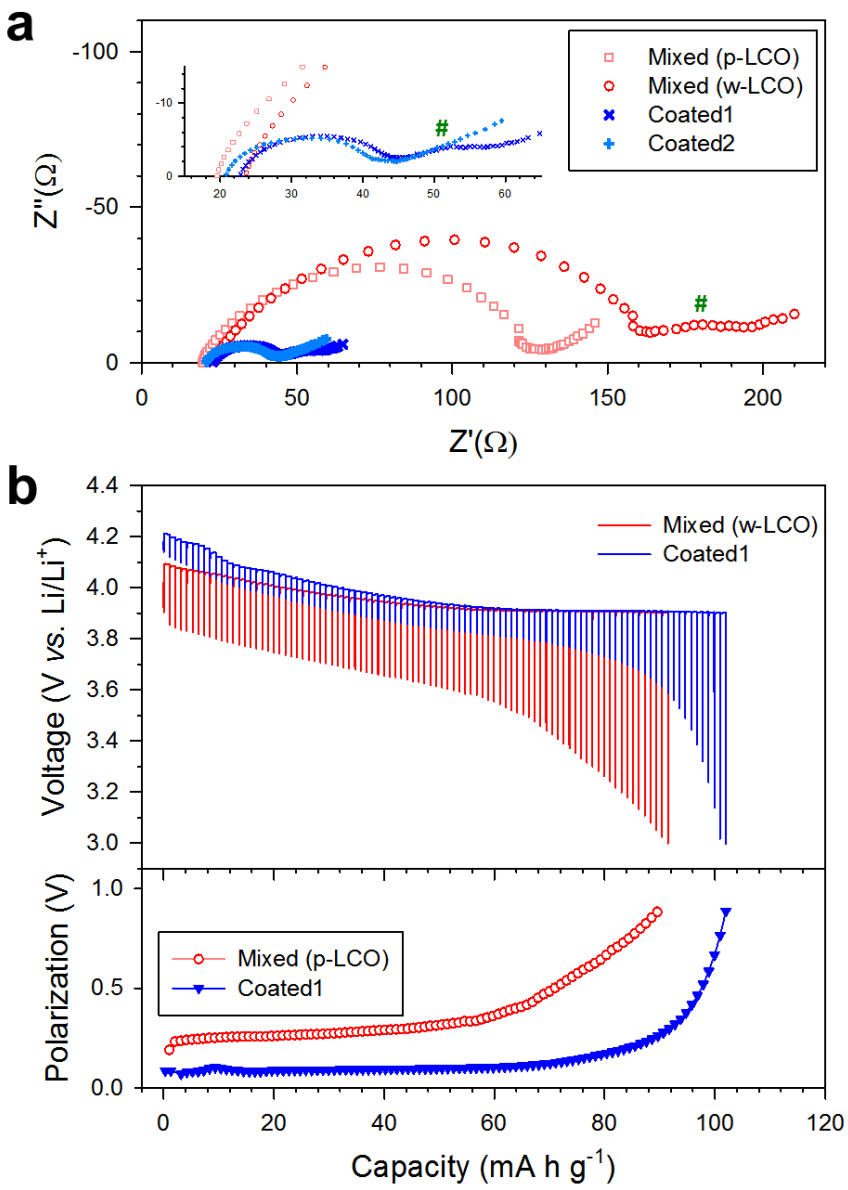

Figure 9. Electrochemical characterization of the mixed electrodes and the LSS-coated $LiCoO_2$ electrode. a) Nyquist plots and b) discharge voltage profiles and their corresponding polarization plots obtained by GITT.

The rate capability of the coated electrode made using 0.4LiI-0.6LSS200 as the coating material is also compared (Supporting Information Figure S7). The performance of the electrode made from $LiCoO_2$ coated with 0.4LiI-0.6LSS200 appears inferior to that made from $LiCoO_2$

coated with LSS320 (Coated1), and comparable to that of the mixed electrode made using p-LCO. Considering the almost identical conductivity values of LSS320 (0.14 mS cm^{-1}) and 0.4LiI-0.6LSS200 (0.10 mS cm^{-1}), the distinct difference in rate capability might originate from the presence of I^- ions. As indicated by the XRD patterns (Figure 2b), LiI exists in segregated domains in 0.4LiI-0.6LSS200. It is expected that LiI decomposes at low voltages, thus negatively affecting the interfaces.[46] Care should be taken, however, when comparing these results with the results for the MeOH-solution-processed SE 0.4LiI-0.6Li_4SnS_4 obtained in our previous work, because it did not form segregated LiI.[2d] It is thought that the electrochemical stability of the I^- ions in the MeOH-solution-processed 0.4LiI-0.6Li_4SnS_4 and pure LiI would be different.

5. Conclusion

In summary, a highly conductive, dry-air-stable, and coatable SE, xLiI-(1-x)Li_4SnS_4, was successfully prepared by a scalable aqueous-solution process. The highest ionic conductivity of 0.1 mS cm^{-1} was achieved for the aqueous-solution-processed Li_4SnS_4 and 0.4LiI-0.6Li_4SnS_4 heat-treated at 320 °C and 200 °C, respectively. The ASLBs employing the Li_4SnS_4-coated $LiCoO_2$ significantly outperformed the conventional mixed electrodes, highlighting the critical importance of intimate ionic contact. The negative effect on interfaces caused by the exposure of $LiCoO_2$ to aqueous solutions was alleviated by using a predissolved Li_4SnS_4 solution. We believe that these results are of importance to the commercialization of high-performance all-solid-state technologies.

6. Supporting information

Raman spectra were obtained with Alpha300R (WITec) using a 532 nm He-Ne laser. The cycle tests using liquid electrolytes were obtained by using 2032-type coin cells. The composite electrodes were prepared by spreading LCO powders (p-LCO or w-LCO), Super P, and poly(vinylidene fluoride) (PVDF) binder (KF1100, Kureha Inc.) on Al foil. The weight ratios of LCO:Super P:PVDF were 90:5:5. Li metal foil was used as both counter and reference electrode.

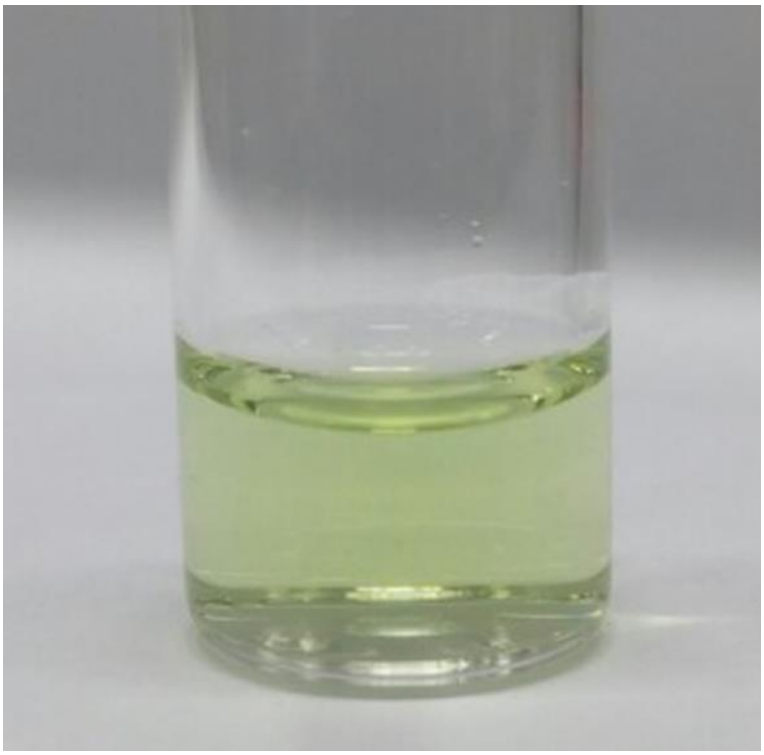

Figure S1. Photograph of the Li_4SnS_4-dissolved aqueous solution.

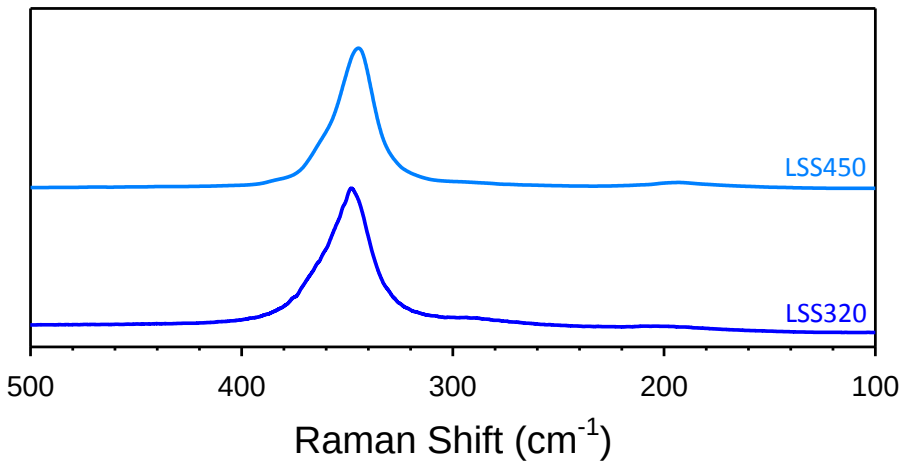

Figure S2. Raman spectra of LSS320 and LSS450.

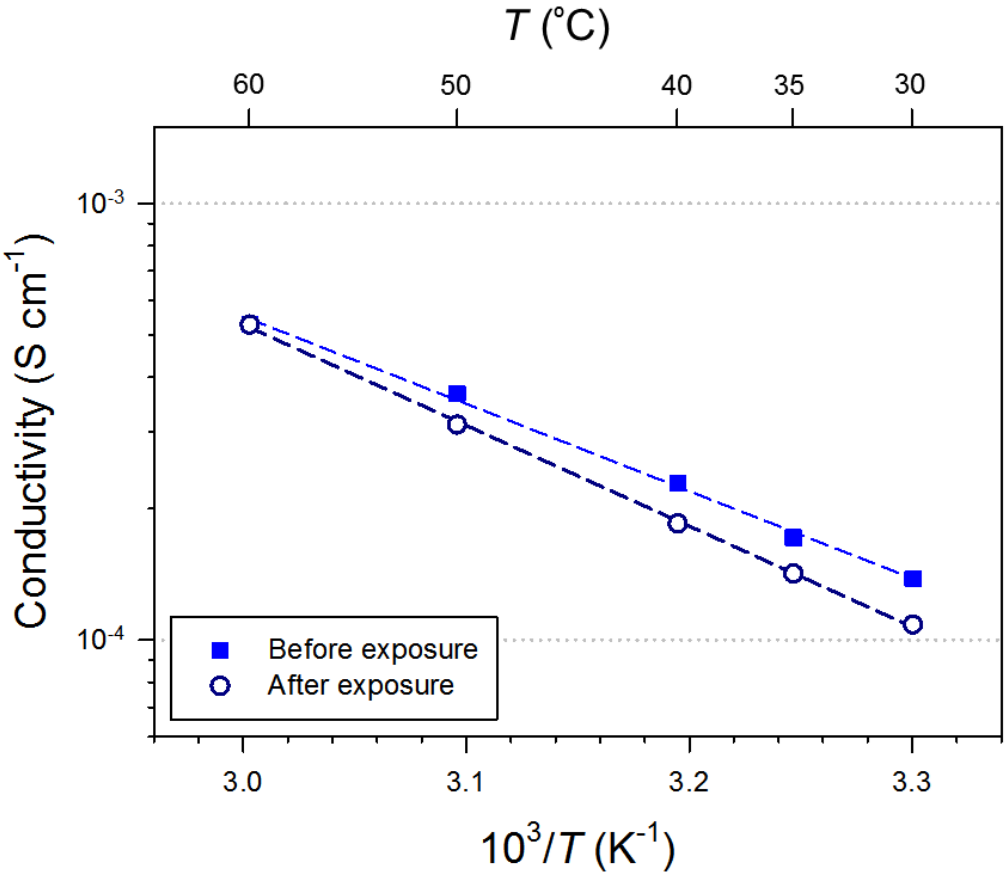

Figure S3. Arrhenius plots of Li ionic conductivity for aqueous-solution processed Li_4SnS_4 powders (LSS320) before and after dry-air exposure.

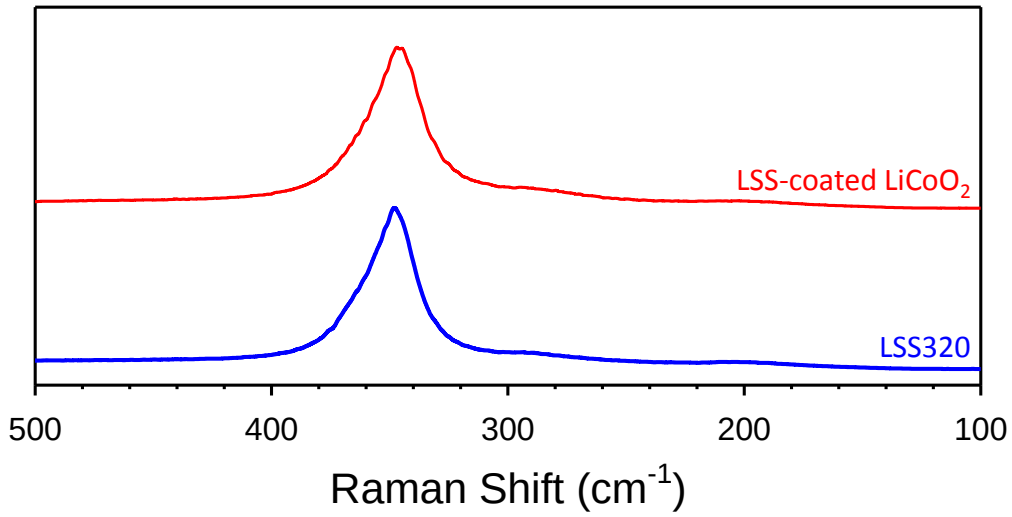

Figure S4. Raman spectra of LSS-coated $LiCoO_2$. The spectra of LSS320 is also shown for comparison.

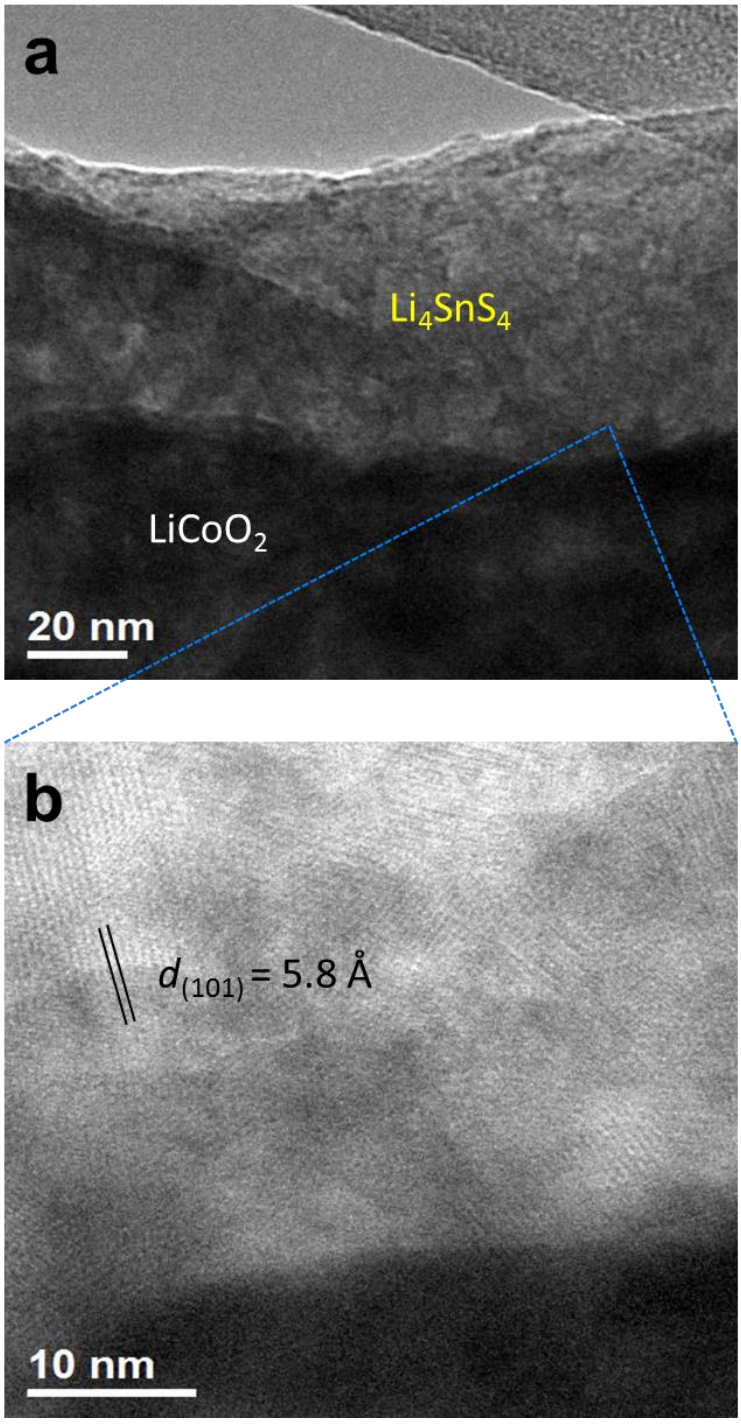

Figure S5. HRTEM images of LSS-coated $LiCoO_2$ particle.

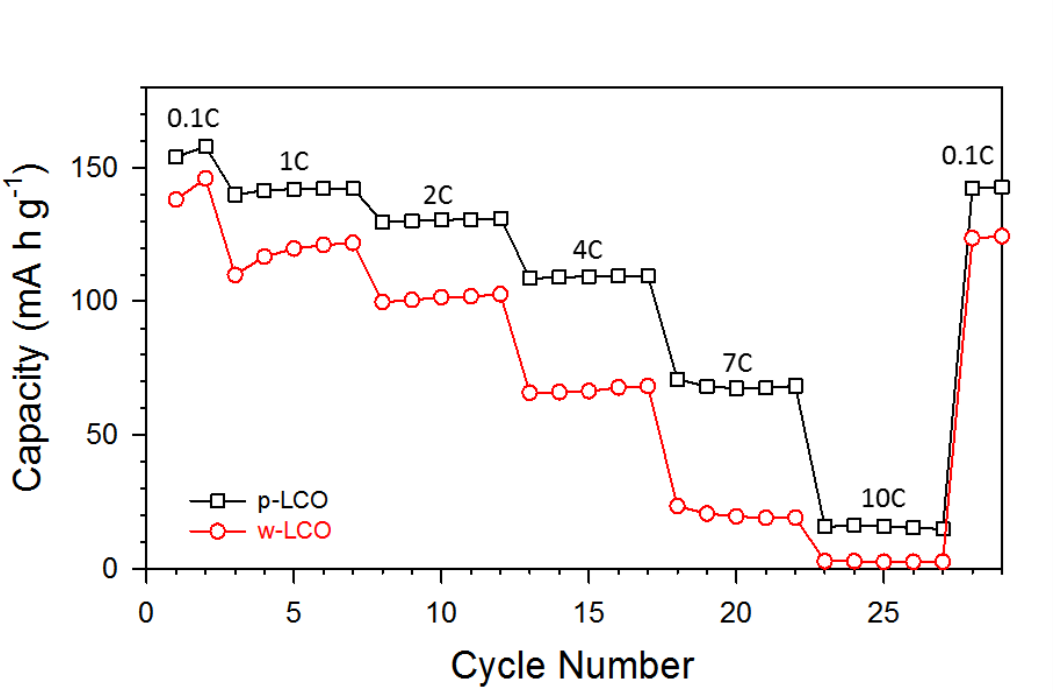

Figure S6. Rate capabilities of p-LCO and w-LCO electrodes in liquid-electrolyte cells cycled between 3.0-4.3 V (vs. Li/Li^+).

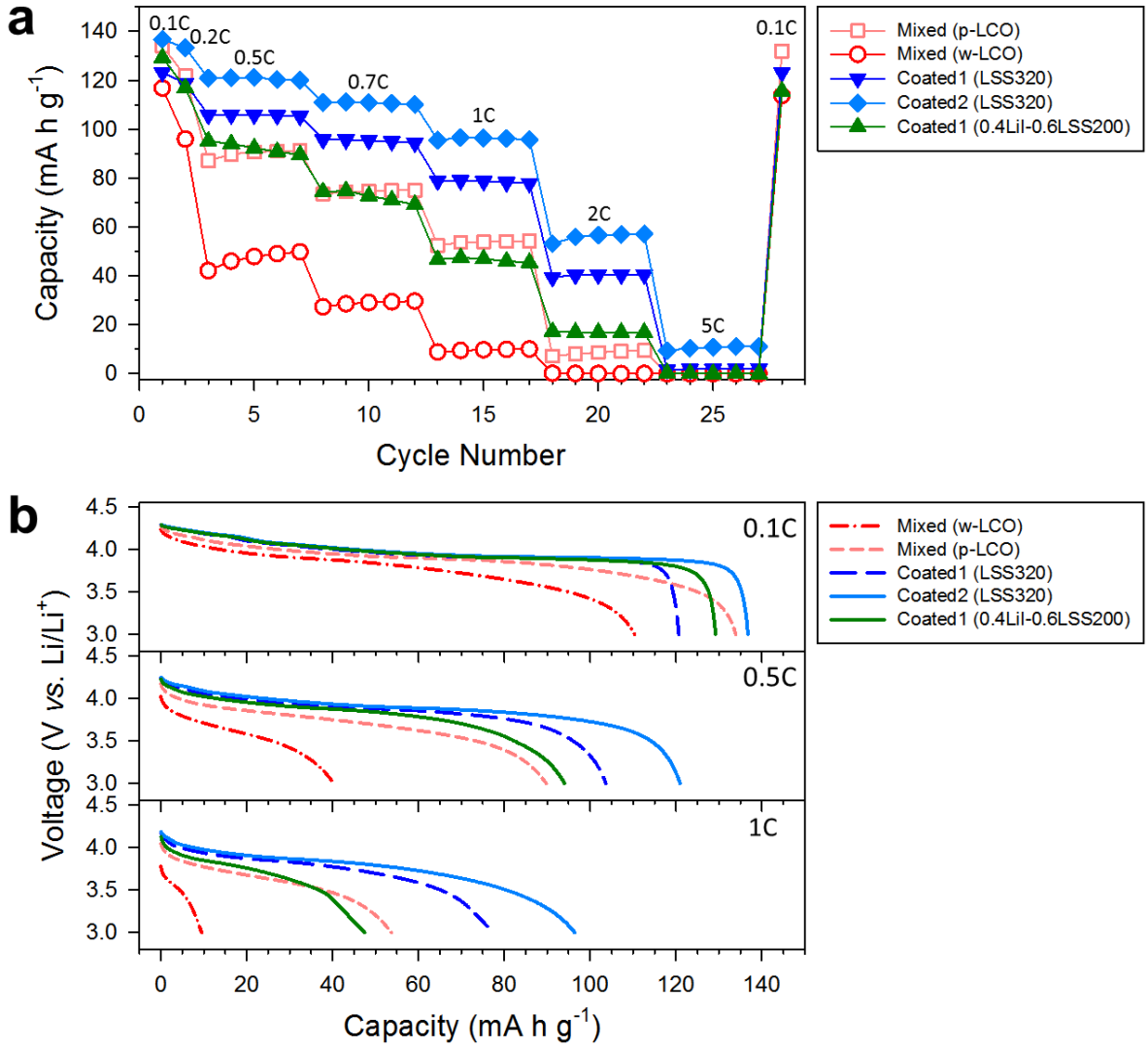

Figure S7. Rate capability of the 0.4LiI-0.6LSS200-coated $LiCoO_2$ electrode. a) Variations in discharge capacities versus charge-discharge cycle number at different C-rates. b) Discharge voltage profiles at different C-rates. The $LiCoO_2$:0.4LiI-0.6LSS200 weight ratio in the composite electrodes was 85:15. The data for the mixed electrodes and the LSS320-coated $LiCoO_2$ electrodes are also shown for comparison

REFERENCES

1. Goodenough, J. B.; Kim, Y., Challenges for Rechargeable Li Batteries. *Chem Mater* **2010,** *22* (3), 587-603.
2. (a) Kamaya, N.; Homma, K.; Yamakawa, Y.; Hirayama, M.; Kanno, R.; Yonemura, M.; Kamiyama, T.; Kato, Y.; Hama, S.; Kawamoto, K.; Mitsui, A., A lithium superionic conductor. *Nat. Mater.* **2011,** *10*, 682-686; (b) Jung, Y. S.; Oh, D. Y.; Nam, Y. J.; Park, K. H., Issues and Challenges for Bulk-Type All-Solid-State Rechargeable Lithium Batteries using Sulfide Solid Electrolytes. *Israel J. Chem.* **2015,** *55*, 472; (c) Janek, J.; Zeier, W. G., A solid future for battery development. *Nat. Energy* **2016**; (d) Park, K. H.; Oh, D. Y.; Choi, Y. E.; Nam, Y. J.; Han, L.; Kim, J.-Y.; Xin, H.; Lin, F.; Oh, S. M.; Jung, Y. S., Solution-Processable Glass LiI-Li_4SnS_4 Superionic Conductors for All-Solid-State Li-Ion Batteries. *Adv. Mater.* **2016,** *28*, 1874-1883; (e) Kato, Y.; Hori, S.; Saito, T.; Suzuki, K.; Hirayama, M.; Mitsui, A.; Yonemura, M.; Iba, H.; Kanno, R., High-power all-solid-state batteries using sulfide superionic conductors. *Nat. Energy* **2016,** *1*, 16030; (f) Wang, Y.; Richards, W. D.; Ong, S. P.; Miara, L. J.; Kim, J. C.; Mo, Y.; Ceder, G., Design principles for solid-state lithium superionic conductors. *Nat. Mater.* **2015,** *14*, 1026.
3. Seino, Y.; Ota, T.; Takada, K.; Hayashi, A.; Tatsumisago, M., A sulphide lithium super ion conductor is superior to liquid ion conductors for use in rechargeable batteries. *Energy Environ. Sci.* **2014,** *7* (2), 627-631.
4. Xu, K., Nonaqueous Liquid Electrolytes for Lithium-Based Rechargeable Batteries. *Chem. Rev.* **2004,** *104*, 4303-4417.
5. Shin, B. R.; Nam, Y. J.; Oh, D. Y.; Kim, D. H.; Kim, J. W.; Jung, Y. S., Comparative Study of TiS_2/Li-In All-Solid-State Lithium Batteries Using Glass-Ceramic Li_3PS_4 and $Li_{10}GeP_2S_{12}$ Solid Electrolytes. *Electrochim. Acta* **2014,** *146*, 395-402.
6. Sakuda, A.; Hayashi, A.; Tatsumisago, M., Interfacial Observation between $LiCoO_2$ Electrode and Li_2S-P_2S_5 Solid Electrolytes of All-Solid-State Lithium Secondary Batteries Using Transmission Electron Microscopy. *Chem. Mater.* **2010,** *22*, 949-956.
7. Haruyama, J.; Sodeyama, K.; Han, L.; Takada, K.; Tateyama, Y., Space-Charge Layer Effect at Interface between Oxide Cathode and Sulfide Electrolyte in All-Solid-State Lithium-Ion Battery. *Chem. Mater.* **2014,** *26* (14), 4248-4255.
8. Oh, D. Y.; Nam, Y. J.; Park, K. H.; Jung, S. H.; Cho, S.-J.; Kim, Y. K.; Lee, Y.-G.; Lee, S.-Y.; Jung, Y. S., Excellent Compatibility of Solvate Ionic Liquids with Sulfide Solid Electrolytes: Toward Favorable Ionic Contacts in Bulk-Type All-Solid-State Lithium-Ion Batteries. *Adv. Energy Mater.* **2015,** *5*, 1500865.
9. Ohta, S.; Seki, J.; Yagi, Y.; Kihira, Y.; Tani, T.; Asoka, T., Co-sinterable lithium garnet-type oxide electrolyte with cathode for all-solid-state lithium ion battery. *J. Power Sources* **2014,** *265*, 40-44.
10. (a) Jeong, S.-K.; Inaba, M.; Iriyarna, Y.; Abe, T.; Ogumi, Z., Interfacial reactions between graphite electrodes and propylene carbonate-based solutions: Electrolyte-concentration dependence of electrochemical lithium intercalation reaction. *J. Power Sources* **2008,** *175* (1), 540-546; (b) Kotobuki, M.; Munakata, H.; Kanamura, K.; Sato, Y.; Yoshida, T., Compatibility of $Li_7La_3Zr_2O_{12}$ Solid Electrolyte to All-Solid-State Battery Using Li Metal Anode. *J. Electrochem. Soc.* **2010,** *157* (10), A1076-A1079.
11. (a) Sakuda, A.; Hayashi, A.; Tatsumisago, M., Sulfide Solid Electrolyte with Favorable Mechanical Property for All-Solid-State Lithium Battery. *Sci. Rep.* **2013,** *3*, 2261; (b) Nam, Y. J.; Jo, S. J.; Oh, D. Y.; Im, J. M.; Kim, S. Y.; Song, J. H.; Lee, Y. G.; Lee, S. Y.; Jung, Y. S., Bendable

and Thin Sulfide Solid Electrolyte Film: A New Electrolyte Opportunity for Free-Standing and Stackable High-Energy All-Solid-State Lithium-Ion Batteries. *Nano Lett.* **2015,** *15*, 3317.
12. Banerjee, A.; Park, K. H.; Heo, J. W.; Nam, Y. J.; Moon, C. K.; Oh, S. M.; Hong, S.-T.; Jung, Y. S., Na_3SbS_4 : A Solution Processable Sodium Superionic Conductor for All-Solid-State Sodium-Ion Batteries. *Angew. Chem. Int. Ed.* **2016,** *55*, 9634.
13. Trevey, J. E.; Stoldt, C. R.; Lee, S. H., High Power Nanocomposite TiS2 Cathodes for All-Solid-State Lithium Batteries. *J Electrochem Soc* **2011,** *158* (12), A1282-A1289.
14. Oh, D. Y.; Choi, Y. E.; Kim, D. H.; Lee, Y. G.; Kim, B. S.; Park, J.; Sohn, H.; Jung, Y. S., All-solid-state lithium-ion batteries with TiS2 nanosheets and sulphide solid electrolytes. *J Mater Chem A* **2016,** *4* (26), 10329-10335.
15. Shin, B. R.; Nam, Y. J.; Kim, J. W.; Lee, Y. G.; Jung, Y. S., Interfacial Architecture for Extra Li+ Storage in All-Solid-State Lithium Batteries. *Sci Rep-Uk* **2014,** *4*.
16. Sakuda, A.; Hayashi, A.; Ohtomo, T.; Hama, S.; Tatsumisago, M., $LiCoO_2$ Electrode Particles Coated With Li_2S-P_2S_5 Solid Electrolyte for All-Solid-State Batteries. *Electrochem. Solid-State Lett.* **2010,** *13* (6), A73-A75.
17. Wang, Y.; Liu, Z.; Zhu, X.; Tang, Y.; Huang, F., Highly lithium-ion conductive thio-LISICON thin film processed by low-temperature solution method. *J. Power Sources* **2013,** *224*, 225-229.
18. Liu, Z.; Fu, W.; Payzant, E. A.; Yu, X.; Wu, Z.; Dudney, N. J.; Kiggans, J.; Hong, K.; Rondinone, A. J.; Liang, C., Anomalous High Ionic Conductivity of Nanoporous beta-Li_3PS_4. *J. Am. Chem. Soc.* **2013,** *135* (3), 975-978.
19. Teragawa, S.; Aso, K.; Tadanaga, K.; Hayashi, A.; Tatsumisago, M., Preparation of Li_2S-P_2S_5 solid electrolyte from N-methylformamide solution and application for all-solid-state lithium battery. *J. Power Sources* **2014,** *248*, 939-942.
20. Rangasamy, E.; Liu, Z.; Gobet, M.; Pilar, K.; Sahu, G.; Zhou, W.; Wu, H.; Greenbaum, S.; Liang, C., An Iodine-Based $Li_7P_2S_8I$ Superionic Conductor. *J. Am. Chem. Soc.* **2015,** *137* (4), 1384-1387.
21. Yubuchi, S.; Teragawa, S.; Aso, K.; Tadanaga, K.; Hayashi, A.; Tatsumisago, M., Preparation of high lithium-ion conducting Li_6PS_5Cl solid electrolyte from ethanol solution for all-solid-state lithium batteries. *J. Power Sources* **2015,** *293*, 941-945.
22. Kaib, T.; Haddadpour, S.; Kapitein, M.; Bron, P.; Schroeder, C.; Eckert, H.; Roling, B.; Dehnen, S., New Lithium Chalcogenidotetrelates, LiChT: Synthesis and Characterization of the Li^+-Conducting Tetralithium ortho-Sulfidostannate Li_4SnS_4. *Chem. Mater.* **2012,** *24* (11), 2211-2219.
23. Sahu, G.; Lin, Z.; Li, J.; Liu, Z.; Dudney, N.; Liang, C., Air-stable, high-conduction solid electrolytes of arsenic-substituted Li_4SnS_4. *Energy Environ. Sci.* **2014,** *7* (3), 1053-1058.
24. Brant, J. A.; Massi, D. M.; Holzwarth, N. A. W.; MacNeil, J. H.; Douvalis, A. P.; Bakas, T.; Martin, S. W.; Gross, M. D.; Aitken, J. A., Fast Lithium Ion Conduction in Li_2SnS_3: Synthesis, Physicochemical Characterization, and Electronic Structure. *Chem. Mater.* **2015,** *27* (1), 189-196.
25. Armand, M.; Tarascon, J. M., Building better batteries. *Nature* **2008,** *451* (7179), 652-657.
26. Bhatt, M. D.; O'Dwyer, C., Recent progress in theoretical and computational investigations of Li-ion battery materials and electrolytes. *Phys Chem Chem Phys* **2015,** *17* (7), 4799-4844.
27. Whittingham, M. S., Lithium batteries and cathode materials. *Chem Rev* **2004,** *104* (10), 4271-4301.
28. Kim, M. G.; Shin, H. J.; Kim, J. H.; Park, S. H.; Sun, Y. K., XAS investigation of inhomogeneous metal-oxygen bond covalency in bulk and surface for charge compensation in li-

ion battery cathode Li[Ni1/3Co1/3Mn1/3]O-2 material. *J Electrochem Soc* **2005,** *152* (7), A1320-A1328.
29. Kim, D.; Yoon, T.; Park, S.; Shin, S.; Ryu, J. H.; Oh, S. M., Re-Deposition of Aluminum Species after Dissolution to Improve Electrode Performances of Lithium Manganese Oxide. *J Electrochem Soc* **2014,** *161* (14), A2020-A2025.
30. Yoon, T.; Kim, D.; Park, K. H.; Park, H.; Jurng, S.; Jang, J.; Ryu, J. H.; Kim, J. J.; Oh, S. M., Compositional Change of Surface Film Deposited on LiNi0.5Mn1.5O4 Positive Electrode. *J Electrochem Soc* **2014,** *161* (4), A519-A523.
31. Xu, W.; Wang, J. L.; Ding, F.; Chen, X. L.; Nasybutin, E.; Zhang, Y. H.; Zhang, J. G., Lithium metal anodes for rechargeable batteries. *Energ Environ Sci* **2014,** *7* (2), 513-537.
32. (a) Tamura, N.; Ohshita, R.; Fujimoto, M.; Kamino, M.; Fujitani, S., Advanced structures in electrodeposited tin base negative electrodes for lithium secondary batteries. *J Electrochem Soc* **2003,** *150* (6), A679-A683; (b) Winter, M.; Besenhard, J. O., Electrochemical lithiation of tin and tin-based intermetallics and composites. *Electrochimica Acta* **1999,** *45* (1-2), 31-50.
33. Stramare, S.; Thangadurai, V.; Weppner, W., Lithium lanthanum titanates: A review. *Chem Mater* **2003,** *15* (21), 3974-3990.
34. Murugan, R.; Thangadurai, V.; Weppner, W., Fast lithium ion conduction in garnet-type Li7La3Zr2O12. *Angew Chem Int Edit* **2007,** *46* (41), 7778-7781.
35. Aono, H.; Sugimoto, E.; Sadaoka, Y.; Imanaka, N.; Adachi, G., Ionic-Conductivity of Solid Electrolytes Based on Lithium Titanium Phosphate. *J Electrochem Soc* **1990,** *137* (4), 1023-1027.
36. Kanno, R.; Maruyama, M., Lithium ionic conductor thio-LISICON - The Li2S-GeS2-P2S5 system. *J Electrochem Soc* **2001,** *148* (7), A742-A746.
37. Sakuda, A.; Kitaura, H.; Hayashi, A.; Tadanaga, K.; Tatsumisago, M., Modification of Interface Between LiCoO2 Electrode and Li2S-P2S5 Solid Electrolyte Using Li2O-SiO2 Glassy Layers. *J Electrochem Soc* **2009,** *156* (1), A27-A32.
38. Ohta, N.; Takada, K.; Zhang, L. Q.; Ma, R. Z.; Osada, M.; Sasaki, T., Enhancement of the high-rate capability of solid-state lithium batteries by nanoscale interfacial modification. *Adv Mater* **2006,** *18* (17), 2226-+.
39. Mucha, M.; Jungwirth, P., Salt crystallization from an evaporating aqueous solution by molecular dynamics simulations. *J. Phys. Chem. B* **2003,** *107* (33), 8271-8274.
40. (a) Liang, C. C., Conduction Characteristics of Lithium Iodide Aluminum Oxide Solid Electrolytes. *J. Electrochem. Soc.* **1973,** *120* (10), 1289-1292; (b) Maier, J., Nanoionics: ion trasport and electrochemical storage in confined systems. *Nat. Mater.* **2005,** *4*, 805-815.
41. (a) Liu, H. S.; Zhang, Z. R.; Gong, Z. L.; Yang, Y., Origin of deterioration for $LiNiO_2$ cathode material during storage in air. *Electrochem. Solid-State Lett.* **2004,** *7* (7), A190-A193; (b) Chen, Z.; Dahn, J. R., Studies of $LiCoO_2$ Coated with Metal Oxides. *Electrochem. Solid-State Lett.* **2003,** *6* (11), A221-A224; (c) Motzko, M.; Solano, M. A. C.; Jaegermann, W.; Hausbrand, R., Photoemission Study on the Interaction Between LiCoO2 Thin Films and Adsorbed Water. *J. Phys. Chem. C* **2015,** *119* (41), 23407-23412.
42. (a) Jung, Y. S.; Lu, P.; Cavanagh, A. S.; Ban, C.; Kim, G. H.; Lee, S. H.; George, S. M.; Harris, S. J.; Dillon, A. C., Unexpected Improved Performance of ALD Coated $LiCoO_2$/Graphite Li-Ion Batteries. *Adv. Energy Mater.* **2013,** *3* (2), 213-219; (b) Tron, A.; Park, Y. D.; Mun, J., AlF_3-coated $LiMn_2O_4$ as cathode material for aqueous rechargeable lithium battery with improved cycling stability. *J. Power Sources* **2016,** *325*, 360-364.
43. Kim, H.; Hong, J.; Park, K.-Y.; Kim, H.; Kim, S.-W.; Kang, K., Aqueous Rechargeable Li and Na Ion Batteries. *Chem. Rev.* **2014,** *114* (23), 11788-11827.

44. (a) Bard, A. J.; Faulkner, L. R., *Electrochemical Methods: Fundamentals and Applications*. John Wiley & Sons, Inc.: New York, 2001; Vol. 2nd; (b) Kang, E.; Jung, Y. S.; Kim, G. H.; Chun, J.; Wiesner, U.; Dillon, A. C.; Kim, J. K.; Lee, J., Highly Improved Rate Capability for a Lithium-Ion Battery Nano-$Li_4Ti_5O_{12}$ Negative Electrode via Carbon-Coated Mesoporous Uniform Pores with a Simple Self-Assembly Method. *Adv. Funct. Mater.* **2011,** *21* (22), 4349-4357; (c) Gaberscek, M.; Moskon, J.; Erjavec, B.; Dominko, R.; Jamnik, J., The Importance of Interfase Contacts in Li Ion Electrodes: The Meaning of the HIgh-Frequency Impedance Arc. *Electrochem. Solid-State Lett.* **2008,** *11* (10), A170-A174.
45. Weppner, W.; Huggins, R. A., Determination of Kinetic-Parameters of Mixed-Conducting Electrodes and Application to System Li_3Sb. *J. Electrochem. Soc.* **1977,** *124* (10), 1569-1578.
46. Lim, H.-D.; Song, H.; Kim, J.; Gwon, H.; Bae, Y.; Park, K.-Y.; Hong, J.; Kim, H.; Kim, T.; Kim, Y. H.; Lepro, X.; Ovalle-Robles, R.; Baughman, R. H.; Kang, K., Superior Rechargeability and Efficiency of Lithium-Oxygen Batteries: Hierarchical Air Electrode Architecture Combined with a Soluble Catalyst. *Angew. Chem. Int. Ed.* **2014,** *53* (15), 3926-3931.